Predictive Hybrid Resource Allocation in Wireless Sensing Systems for Value of Service Maximization

Biwei Li* {biwei.li@seu.edu.cn} and Wanli Zhang‡ {wanli.zhang@ntu.edu.sg}
* School of Computer Science and Engineering, Southeast University, Nanjing, China
‡ School of Physical and Mathematical Science, Nanyang Technological University, Singapore

***Abstract*—Wireless sensing has emerged as a key enabling technology for Integrated Sensing and Communication (ISAC) systems, where radio resources are jointly utilized for environmental sensing and communication. However, under limited radio resources, continuously improving sensing accuracy may lead to inefficient resource utilization once the sensing requirement has been satisfied. To address this issue, this paper proposes a Predictive Marginal Value of Sensing (PM-VoS) based resource allocation framework for dynamic wireless sensing systems. The proposed PM-VoS evaluates the long-term marginal utility of current sensing actions by propagating sensing and non-sensing covariance states over a finite prediction horizon. Based on this metric, a hybrid resource allocation algorithm is developed by combining analytical one-step VoS evaluation with learning-assisted residual predictive value estimation. Simulation results in multi-user multi-target scenarios demonstrate that the proposed scheme reduces sensing position error and improves radio resource utilization efficiency compared with non-predictive VoS-based, heuristic, and random allocation methods.**

***Keywords*—Wireless sensing, value of service (VoS), hybrid resource allocation.**

I. Introduction

The proliferation of Internet-of-Things (IoT) applications, including intelligent transportation, industrial automation, and environmental monitoring, has created increasing demand for continuous environmental sensing [1], [2]. Wireless sensing addresses this demand by utilizing radio signals to estimate target states such as position and velocity. With dense deployments of base stations, access points, and local wireless networks, sensing functions can be supported by existing wireless infrastructures without requiring dedicated sensing devices [3]. However, wireless sensing shares limited radio resources with communication services. Consequently, continuously improving sensing performance may lead to inefficient resource utilization, particularly when sensing requirements have already been satisfied.

Accurate wireless sensing consumes substantial radio resources, including sensing power, bandwidth, and time-frequency resource blocks. Under limited radio resources, efficient sensing resource allocation becomes critical in multi-user multi-target sensing systems. Existing sensing-oriented allocation schemes mainly optimize sensing accuracy or uncertainty reduction [4]. However, continuously improving sensing accuracy may result in inefficient resource utilization once the required sensing quality has already been achieved.

To address this issue, the concept of Value of Service (VoS) has been introduced to characterize the utility of sensing performance from a user-demand-oriented perspective [5], [6]. Instead of directly optimizing absolute sensing accuracy, VoS maps sensing uncertainty to sensing utility according to user-specific sensing requirements. Nevertheless, conventional VoS-based allocation is typically based on instantaneous sensing utility or one-step uncertainty reduction [7], which may be insufficient for dynamic sensing systems. Authors in [8] proposed a beamforming optimization strategy to achieve dynamic tracking. [9] introduced a movable intelligent surface for higher signal to noise ratio in wireless sensing. However, most existing studies evaluate sensing value only within a single time slot, ignoring its long-term impact on future tracking performance. Due to target mobility and time-varying channel conditions, future sensing uncertainty may evolve significantly even when the current sensing quality is satisfactory. Therefore, resource allocation decisions should account not only for immediate sensing utility, but also for the long-term impact of current sensing actions on future sensing performance.

To address the above limitation, this paper proposes a Predictive Marginal Value of service (PM-VoS) based resource allocation framework for dynamic wireless sensing systems. The proposed PM-VoS quantifies the long-term marginal sensing utility of current sensing actions by jointly propagating sensing-enabled and sensing-disabled covariance states over a finite prediction horizon. In this way, the proposed metric captures the future evolution of sensing uncertainty rather than relying only on instantaneous sensing gain. Based on the proposed PM-VoS, a hybrid resource allocation algorithm is developed by combining analytical one-step VoS evaluation with learning-assisted predictive utility estimation. The proposed algorithm allocates limited radio resources according to both predictive sensing utility and resource consumption, thereby enabling efficient long-term sensing resource allocation under dynamic wireless sensing environments.

The remainder of this paper is organized as follows. Section II introduces the system model and formulates the resource allocation problem. Section III develops the predictive hybrid resource allocation algorithm. Simulation results are presented in Section IV, followed by the conclusion in Section V.

II. System Model

A. Signal Model

We consider a bistatic mmWave multiple-input multiple-output (MIMO) orthogonal frequency-division multiplexing

(OFDM) sensing system consisting of one base station(BS), multiple users, and multiple sensing targets. The BS is equipped with N_t transmit antennas and transmits OFDM signals for target tracking. Each user is equipped with N_r receive antennas and receives the target-reflected signal. The set of users is denoted by $\mathcal{K} = \{1, \dots, K\}$, where user k is associated with one sensing target.

Let N and G represent the numbers of subcarriers and OFDM symbols within one sensing slot, respectively. The BS transmits the precoded signal $\mathbf{F}_{g,n}\mathbf{s}_{g,n}$, where $\mathbf{F}_{g,n} \in \mathbb{C}^{N_t \times M_t}$ is the transmit precoding matrix and $\mathbf{s}_{g,n} \in \mathbb{C}^{M_t}$ is the transmitted symbol vector where M_t is the symbol length. For the target-reflected path associated with user k, the MIMO sensing channel on subcarrier n and OFDM symbol g is modeled as [10]

$$\mathbf{H}_{k,t}^{(g)}[n]=\beta_{k,t}e^{-j2\pi n\Delta f\tau_{k,t}}e^{j2\pi gT_{\mathrm{sym}}\nu_{k,t}}\mathbf{a}_r(\theta_{k,t})\mathbf{a}_t^H(\phi_{k,t}) \,, \quad (1)$$

where $\beta_{k,t}$ is the complex reflection coefficient including target reflection and path loss, Δf is the subcarrier spacing, T_{sym} is the OFDM symbol duration, $\tau_{k,t}$ is the bistatic delay, $\nu_{k,t}$ is the bistatic Doppler shift, $\phi_{k,t}$ is the angle of departure (AoD) at the BS, and $\theta_{k,t}$ is angle of arrival (AoA) at user k.

The received signal at user k is therefore given by

$$\mathbf{y}_{k,t}^{(g)}[n] = \mathbf{H}_{k,t}^{(g)}[n]\mathbf{F}_{g,n}\mathbf{s}_{g,n} + \mathbf{n}_{k,t}^{(g)}[n], \quad (2)$$

where $\mathbf{n}_{k,t}^{(g)}[n] \sim \mathcal{CN}(\mathbf{0}, \sigma_n^2\mathbf{I}_{N_r})$ denotes the additive white Gaussian noise (AWGN).

B. Motion Model

The positions of the BS and user k are denoted by $\mathbf{p}_{\mathrm{BS}} = [x_{\mathrm{BS}}, y_{\mathrm{BS}}]^T$ and $\mathbf{p}_{u,k} = [x_{u,k}, y_{u,k}]^T$, respectively. The state of target k at time slot t is $\mathbf{x}_{k,t} = [\mathbf{p}_{k,t}^T, \mathbf{v}_{k,t}^T]^T$, where its position and velocity are denoted by $\mathbf{p}_{k,t} = [x_{k,t}, y_{k,t}]^T$ and $\mathbf{v}_{k,t} = [v_{x,k,t}, v_{y,k,t}]^T$, respectively.

The geometry-dependent sensing parameters of target k are given by

$$\begin{cases} d_{\mathrm{B},k,t} = \left\|\mathbf{p}_{k,t} - \mathbf{p}_{\mathrm{BS}}\right\|, d_{\mathrm{U},k,t} = \left\|\mathbf{p}_{k,t} - \mathbf{p}_{u,k}\right\|, \\ \rho_{k,t} = d_{\mathrm{B},k,t} + d_{\mathrm{U},k,t}, \tau_{k,t} = \dfrac{\rho_{k,t}}{c}, \\ \phi_{k,t} = \operatorname{atan2}\left(y_{k,t} - y_{\mathrm{BS}}, x_{k,t} - x_{\mathrm{BS}}\right), \\ \theta_{k,t} = \operatorname{atan2}\left(y_{k,t} - y_{u,k}, x_{k,t} - x_{u,k}\right), \end{cases} \quad (3)$$

where $d_{\mathrm{B},k,t}$, $d_{\mathrm{U},k,t}$ are the distance between BS and target, target and user, respectively. The bistatic range rate is obtained by differentiating the bistatic propagation distance $\rho_{k,t}$ with respect to time

$$\dot{\rho}_{k,t} = \frac{d\rho_{k,t}}{dt} = \mathbf{v}_{k,t}^T\left(\frac{\mathbf{p}_{k,t} - \mathbf{p}_{\mathrm{BS}}}{d_{\mathrm{B},k,t}} + \frac{\mathbf{p}_{k,t} - \mathbf{p}_{u,k}}{d_{\mathrm{U},k,t}}\right). \quad (4)$$

The corresponding Doppler shift is modeled as

$$\nu_{k,t} = \frac{f_c}{c}\dot{\rho}_{k,t}, \quad (5)$$

where the sign convention follows the adopted complex baseband representation.

The target mobility is modeled by a quasi-constant velocity model [11]

$$\mathbf{x}_{k,t+1} = \mathbf{F}\mathbf{x}_{k,t} + \mathbf{w}_{k,t}, \quad (6)$$

where $\mathbf{w}_{k,t}$ is the process noise with covariance matrix $\mathbf{Q}_k$, and

$$\mathbf{F} = \begin{bmatrix} 1 & 0 & \Delta t & 0 \\ 0 & 1 & 0 & \Delta t \\ 0 & 0 & 1 & 0 \\ 0 & 0 & 0 & 1 \end{bmatrix}, \quad (7)$$

where Δt is the time interval between two time slots.

The estimation parameters $\mathbf{z}_{k,t} = [\tau_{k,t}, \nu_{k,t}, \phi_{k,t}, \theta_{k,t}]^T$ can be extracted from the received MIMO-OFDM signal using parameter estimation methods such as compressive sensing [10]. Herein, we adopt a simplified observation model with estimator $\hat{h}_k$. Since $\mathbf{z}_{k,t}$ are determined by the target state through the bistatic geometry, the measurement model is

$$\mathbf{z}_{k,t} = \hat{h}_k(\mathbf{x}_{k,t}) + \mathbf{e}_{k,t}, \quad (8)$$

where $\mathbf{e}_{k,t}$ represents the effective parameter estimation error.

Let $P_{k,t}$ and $B_{k,t}$ denote the sensing power and sensing bandwidth allocated to target k at time slot t. The measurement error covariance is modeled as

$$\mathbf{R}_{k,t}(P_{k,t}, B_{k,t}) = \operatorname{diag}\left(\sigma_{\tau,k,t}^2, \sigma_{\nu,k,t}^2, \sigma_{\phi,k,t}^2, \sigma_{\theta,k,t}^2\right). \quad (9)$$

Following Cramér–Rao lower bound (CRLB) sensing error models [6], the measurement error variances are modeled as

$$\begin{cases} \sigma_{\tau,k,t}^2 = \dfrac{c_\tau}{B_{k,t}^2\mathrm{SNR}_{k,t}}, \\ \sigma_{\nu,k,t}^2 = \dfrac{c_\nu}{T_{\mathrm{obs}}^2\mathrm{SNR}_{k,t}}, \\ \sigma_{\phi,k,t}^2 = \dfrac{c_\phi}{N_t(N_t^2 - 1)\mathrm{SNR}_{k,t}}, \\ \sigma_{\theta,k,t}^2 = \dfrac{c_\theta}{N_r(N_r^2 - 1)\mathrm{SNR}_{k,t}}, \end{cases} \quad (10)$$

where c_τ, c_ν, c_ϕ, and c_θ are positive scaling constants, and $T_{\mathrm{obs}} = GT_{\mathrm{sym}}$ denotes the coherent observation time within one sensing slot.

The effective sensing signal to noise ratio (SNR) is [6]

$$\mathrm{SNR}_{k,t} = \frac{P_{k,t}B_{k,t}G_{k,t}}{N_0}, \quad (11)$$

where $G_{k,t}$ denotes the effective bistatic channel gain and N_0 is the noise power spectral density.

At the time slot t, the extended Kalman filter (EKF) prediction model gives

$$\hat{\mathbf{x}}_{k,t|t-1} = \mathbf{F}\hat{\mathbf{x}}_{k,t-1|t-1}, \quad (12)$$

and

$$\mathbf{P}_{k,t|t-1} = \mathbf{F}\mathbf{P}_{k,t-1|t-1}\mathbf{F}^T + \mathbf{Q}_k. \quad (13)$$

When a sensing resource block $(P_{k,t}, B_{k,t})$ is assigned to target k, the predicted covariance is updated using the EKF update step, where $\mathbf{J}_{k,t} = \left.\frac{\partial h_k(\mathbf{x})}{\partial \mathbf{x}}\right|_{\mathbf{x}=\hat{\mathbf{x}}_{k,t|t-1}}$ denotes the

Jacobian matrix of the sensing observation function evaluated at the predicted state. The innovation covariance is

$$\mathbf{S}_{k,t} = \mathbf{J}_{k,t}\mathbf{P}_{k,t|t-1}\mathbf{J}_{k,t}^T + \mathbf{R}_{k,t}(P_{k,t}, B_{k,t}), \tag{14}$$

and the Kalman gain is

$$\mathbf{K}_{k,t} = \mathbf{P}_{k,t|t-1}\mathbf{J}_{k,t}^T\mathbf{S}_{k,t}^{-1}. \tag{15}$$

The posterior covariance after sensing is

$$\mathbf{P}_{k,t|t}^{\mathrm{s}} = \left(\mathbf{I} - \mathbf{K}_{k,t}\mathbf{J}_{k,t}\right)\mathbf{P}_{k,t|t-1}. \tag{16}$$

If target k is not sensed at time slot t, the posterior covariance remains $\mathbf{P}_{k,t|t}^{\mathrm{ns}} = \mathbf{P}_{k,t|t-1}$.

C. Predictive Sensing Model

To characterize the long-term impact of the current sensing decision, we propagate the covariance evolution under both sensing and non-sensing cases over a prediction horizon of L time slots. For $\ell = 1, \ldots, L$, the future covariance under the sensing case is

$$\mathbf{P}_{k,t+\ell|t}^{\mathrm{s}} = \mathbf{F}^\ell\mathbf{P}_{k,t|t}^{\mathrm{s}}\left(\mathbf{F}^\ell\right)^T + \sum_{i=0}^{\ell-1}\mathbf{F}^i\mathbf{Q}_k\left(\mathbf{F}^i\right)^T. \tag{17}$$

The future covariance under the non-sensing case is

$$\mathbf{P}_{k,t+\ell|t}^{\mathrm{ns}} = \mathbf{F}^\ell\mathbf{P}_{k,t|t}^{\mathrm{ns}}\left(\mathbf{F}^\ell\right)^T + \sum_{i=0}^{\ell-1}\mathbf{F}^i\mathbf{Q}_k\left(\mathbf{F}^i\right)^T. \tag{18}$$

The predicted target position error is defined as the trace of the position covariance submatrix. Under the sensing case, it is given by

$$u_{k,t+\ell}^{\mathrm{s}} = \mathrm{tr}\left(\mathbf{E}\mathbf{P}_{k,t+\ell|t}^{\mathrm{s}}\mathbf{E}^T\right), \tag{19}$$

where

$$\mathbf{E} = \begin{bmatrix} 1 & 0 & 0 & 0 \\ 0 & 1 & 0 & 0 \end{bmatrix} \tag{20}$$

selects the position components from the target state. Under the non-sensing case, there is

$$u_{k,t+\ell}^{\mathrm{ns}} = \mathrm{tr}\left(\mathbf{E}\mathbf{P}_{k,t+\ell|t}^{\mathrm{ns}}\mathbf{E}^T\right). \tag{21}$$

Assueme each user is associated with a target-specific sensing accuracy requirement, denoted by $\epsilon_k^{\mathrm{req}}$. The sensing satisfaction of user k is modeled as [5], [6]

$$V_k(u) = \frac{1}{1 + \exp\left[\alpha_v\left(\frac{u}{\epsilon_k^{\mathrm{req}}} - 1\right)\right]}, \tag{22}$$

where $\alpha_v > 0$ indicates the sharpness of the transition around the required uncertainty level. Once the sensing requirement is satisfied, further improvement in sensing accuracy contributes limited value.

The PM-VoS is defined as the discounted future satisfaction improvement obtained by assigning sensing resource $(P_{k,t}, B_{k,t})$ to target k at time slot t

$$\text{PM-VoS}_{k,t}^{(L)} = \sum_{\ell=1}^{L}\gamma^{\ell-1}\left[V_k\left(u_{k,t+\ell}^{\mathrm{s}}\right) - V_k\left(u_{k,t+\ell}^{\mathrm{ns}}\right)\right], \tag{23}$$

where $\gamma \in (0, 1]$ is a discount factor. Compared with V_k, the PM-VoS measures the long-term marginal benefit of current sensing.

D. Problem Formulation

At each time slot t, the BS allocates sensing power and bandwidth to users for tracking their associated targets. The resource allocation problem is formulated as maximizing the total PM-VoS

$$\mathbf{P1}: \quad \max_{\{P_{k,t}, B_{k,t}\}} \quad \sum_{k=1}^{K}\text{PM-VoS}_{k,t}^{(L)}\left(P_{k,t}, B_{k,t}\right) \tag{24}$$

$$\text{s.t.} \quad \sum_{k=1}^{K} P_{k,t} \leq P_{\mathrm{tot}}, \tag{24a}$$

$$\sum_{k=1}^{K} B_{k,t} \leq B_{\mathrm{tot}}, \tag{24b}$$

$$P_{k,t} \geq 0, \quad B_{k,t} \geq 0, \quad \forall k \in \mathcal{K}. \tag{24c}$$

Constraints (24a) and (24b) impose the total sensing power and bandwidth budgets, respectively, while (24c) ensures non-negative resource allocation. The main challenge is that the sensing value depends not only on the current sensing SNR, but also on how the allocated resources affect future tracking uncertainty. Specifically, $(P_{k,t}, B_{k,t})$ determines the measurement covariance $\mathbf{R}_{k,t}(P_{k,t}, B_{k,t})$, which further affects the posterior covariance and its future propagation. Therefore, the user with the largest current uncertainty is not necessarily the most valuable one to sense; instead, resources should be allocated to users whose future tracking performance benefits most from current sensing.

III. Predictive Hybrid Resource Allocation

To solve the PM-VoS maximization problem in $\mathbf{P1}$, we propose a predictive hybrid resource allocation that combines learning-based predictive value estimation with adaptive value-guided resource allocation. The analytical model provides an one-step sensing value, while the learning model estimates the residual future value.

A. Learning-based Predictive Value Estimation

For user k at time slot t, the analytical one-step marginal VoS is defined as

$$\Delta V_{k,t}^{(1)} = V_k\left(u_{k,t+1}^{\mathrm{s}}\right) - V_k\left(u_{k,t+1}^{\mathrm{ns}}\right). \tag{25}$$

This term measures the immediate sensing benefit after assigning the resource pair to user k. However, it does not fully capture the accumulated future benefit over the prediction horizon. Therefore, we define the residual predictive value as

$$r_{k,t}^{(L)} = \text{PM-VoS}_{k,t}^{(L)} - \Delta V_{k,t}^{(1)}. \tag{26}$$

The residual term represents the future sensing value beyond the one-step marginal VoS. A larger residual reflects the additional long-term tracking value contributed by the current sensing action, while a negligible residual indicates that the sensing benefit is mainly captured by one-step marginal VoS.

For each user, we construct a feature vector

$$\begin{aligned}\mathbf{q}_{k,t} = &[u_{k,t}, \epsilon_k^{\mathrm{req}}, V_k(u_{k,t}), d_{\mathrm{B},k,t}, d_{\mathrm{U},k,t}, \rho_{k,t}, |\dot{\rho}_{k,t}|, \\ &G_{k,t}, \mathrm{SNR}_{k,t}, \mathrm{tr}(\mathbf{Q}_k), \|\hat{\mathbf{v}}_{k,t}\|, P_{k,t}, B_{k,t}]^T,\end{aligned} \tag{27}$$

The feature vector includes the current tracking uncertainty, the user-specific accuracy requirement, the bistatic geometry, the effective sensing channel condition, the target mobility information, and the candidate resources.

A supervised regression model [12] is then trained to approximate the residual predictive value $\hat{r}_{k,t}^{(L)}(P_{k,t}, B_{k,t}) = f_{\boldsymbol{\Theta}}(\mathbf{q}_{k,t})$, where $f_{\boldsymbol{\Theta}}(\cdot)$ denotes the learning model with trainable parameters $\boldsymbol{\Theta}$. The training label is generated by the EKF-based PM-VoS model

$$y_{k,t} = r_{k,t}^{(L)}(P_{k,t}, B_{k,t}). \tag{28}$$

The learning objective is given by

$$\min_{\boldsymbol{\Theta}} \frac{1}{|\mathcal{D}|} \sum_{(\mathbf{q}_{k,t}, y_{k,t}) \in \mathcal{D}} \left| f_{\boldsymbol{\Theta}}(\mathbf{q}_{k,t}) - y_{k,t} \right|^2, \tag{29}$$

where $\mathcal{D}$ is the offline generated training dataset.

Based on the analytical one-step marginal VoS and the learned residual predictive value, the hybrid value score is defined as

$$\Gamma_{k,t} = \Delta V_{k,t}^{(1)} + \lambda \hat{r}_{k,t}^{(L)}, \tag{30}$$

where $\lambda \geq 0$ controls the contribution of the learned predictive correction. When $\lambda = 0$, the score reduces to the one-step marginal VoS. When $\lambda > 0$, the score incorporates the learned future sensing value.

B. VoS-guided Resource Allocation

To reduce the online search complexity, the continuous resource space is discretized into a finite set of power-bandwidth resource blocks

$$\mathcal{R} = \{r_m = (P_m, B_m) \mid m = 1, \ldots, M\}. \tag{31}$$

For user k and resource block r_m, (30) is rewritten as $\Gamma_{k,t}^{(m)} = \Delta V_{k,t}^{(1)} + \lambda f_{\boldsymbol{\Theta}}\left(\mathbf{q}_{k,t}^{(m)}\right)$, where $\mathbf{q}_{k,t}^{(m)}$ is the feature vector constructed using block r_m.

To balance the predicted VoS against the required resource cost, each feasible user-resource pair is ranked by the following value-to-cost ratio $\Psi_{k,t}^{(m)} = \frac{\Gamma_{k,t}^{(m)}}{\eta_P P_m + \eta_B B_m + \epsilon_0}$, where η_P and η_B normalize the power and bandwidth costs, and ϵ_0 is a small positive constant. As a result, resource blocks are allocated according to their value efficiency, rather than their absolute predictive value alone.

At each allocation step, the BS selects the feasible user-resource pair with the largest normalized value utility

$$(k^*, m^*) = \arg \max_{k \in \mathcal{K},\, m \in \mathcal{M}_t} \Psi_{k,t}^{(m)}, \tag{32}$$

where $\mathcal{M}_t$ denotes the set of resource blocks satisfying the remaining power and bandwidth constraints. After assigning r_{m^*} to user k^*, the remaining resources are updated as

$$P_{\text{rem}} \leftarrow P_{\text{rem}} - P_{m^*}, \quad B_{\text{rem}} \leftarrow B_{\text{rem}} - B_{m^*}. \tag{33}$$

The covariance of the selected target is then updated using the EKF sensing update. This procedure is repeated until no feasible resource block remains.

The VoS-guided selection rule acts as a non-learning interface between predictive value estimation and resource allocation. The learning model estimates the residual future value, while the adaptive heuristic determines how to spend the limited power and bandwidth budgets. This hybrid design preserves the interpretability of marginal-value allocation while improving its ability to account for future sensing benefit.

The proposed predictive hybrid resource allocation algorithm consists of an offline training stage and an online allocation stage. In the offline stage, the EKF-based model generates PM-VoS labels for different users, time slots, and candidate resource blocks. The residual predictive value is then obtained according to (26), and the learning model is trained by minimizing (29). In the online stage, the trained model predicts the residual future value for each feasible user-resource pair. The final allocation score is computed, and the adaptive selection rule in (32) is applied sequentially under the remaining resource constraints. The complete procedure is summarized in Algorithm 1.

Algorithm 1: Predictive hybrid resource allocation

Offline training
Generate training samples by simulating user trajectories, candidate resource blocks, and EKF-based covariance evolution.
for each training sample (k, t, m) **do**
  Construct $\mathbf{q}_{k,t}^{(m)}$ using (27).
  Compute $\Delta V_{k,t}^{(1)}$ and $\text{PM-VoS}_{k,t}^{(L)}$ using (25) and the EKF look-ahead model.
  Obtain the residual label $r_{k,t}^{(L)}$ using (26).
end for
Train $f_{\boldsymbol{\Theta}}(\cdot)$ by minimizing (29).
Online allocation
for each time slot t **do**
  Initialize $P_{\text{rem}} = P_{\text{tot}}$ and $B_{\text{rem}} = B_{\text{tot}}$.
  while feasible resource blocks remain **do**
    Evaluate $\Gamma_{k,t}^{(m)}$ and $\Psi_{k,t}^{(m)}$ for all feasible user-resource pairs.
    Select $(k^\star, m^\star)$ according to (32).
    Allocate r_{m^*} to user k^* and update the remaining resources.
    Update the covariance of target $k^\star$ using the EKF sensing update.
  end while
end for

C. Complexity Analysis

The complexity is analyzed in terms of the number of users K, candidate resource blocks M, prediction horizon L, and online allocation rounds I_t. In the offline stage, PM-VoS label generation requires L-step EKF covariance propagation for each user-resource candidate, leading to a complexity of $\mathcal{O}(KML)$ per time slot and $\mathcal{O}(N_{\text{ep}}TKML)$ for N_{ep} training episodes with T slots. This stage also requires storage of the generated feature-label pairs and training of the residual predictive model, which can be performed at the BS or an edge server before deployment. Since this stage is performed offline, it does not affect the real-time allocation cost. In the online stage, each allocation round evaluates all feasible user-resource pairs. With a fixed target state dimension and a lightweight residual predictor, each pair has constant evaluation cost, yielding $\mathcal{O}(KM)$ complexity per round and $\mathcal{O}(I_tKM)$ per time slot. The online resource needs mainly include storing the trained model parameters and evaluating the residual predictor for each feasible pair. Compared with direct online PM-VoS evaluation, which requires $\mathcal{O}(I_tKML)$ due to long-horizon covariance propagation, the proposed method reduces the online complexity to $\mathcal{O}(I_tKM)$ by replacing the repeated look-ahead evaluation with learned residual predictor.

It is worth noting that the offline generated dataset may not fully cover all real-world mobility, channel, and sensing-demand conditions. Therefore, the residual predictor should be trained with sufficiently diverse simulated scenarios and can be periodically updated using newly collected sensing data to reduce distribution mismatch in practical deployments.

IV. Simulation Results

In this section, the effectiveness of the proposed predictive hybrid resource allocation scheme is evaluated through numerical simulations. All simulations are performed in in MATLAB R2025b on a macOS Monterey laptop with an Apple M1 processor and 8 GB memory. We consider a two-dimensional multi-target sensing scenario, as shown in Fig. 1, where one BS is located at the origin and four users are fixed at different positions. Each user is associated with one moving sensing target. The sensing targets move within a $240\text{ m} \times 230\text{ m}$ area following curved stochastic trajectories generated by a quasi-constant velocity model with random acceleration perturbations. The number of users and sensing targets is set to $K = 4$, and the number of time slots is $T = 150$ with a slot duration of $\Delta t = 1$ s. The BS and users are equipped with $N_t = 16$ and $N_r = 8$ antennas, respectively. The carrier frequency is set to $f_c = 28$ GHz. The prediction horizon of the PM-VoS model is set to $L = 10$, and the discount factor is set to $\gamma = 0.9$. The radio resource budget is represented by the number of available radio resource blocks, which varies from 10 to 100. The resource utilization efficiency is evaluated as $\eta_{\text{eff}} = \frac{1}{e_{k,t} \cdot N_{\text{RB}}}$, where N_{RB} denotes the number of radio resource blocks. This metric reflects how efficiently each scheme converts limited radio resources into sensing accuracy improvement.

We compare the proposed method with four schemes. Scheme 1 is the proposed predictive hybrid resource allocation scheme. Scheme 2 is a non-predictive VoS-based allocation scheme that only uses the one-step marginal VoS without future-value correction. Scheme 3 is a heuristic allocation scheme based on the particle swarm optimization (PSO) algorithm [13]. Scheme 4 is a random allocation baseline, where feasible resource blocks are randomly assigned to users under the same total resource constraint.

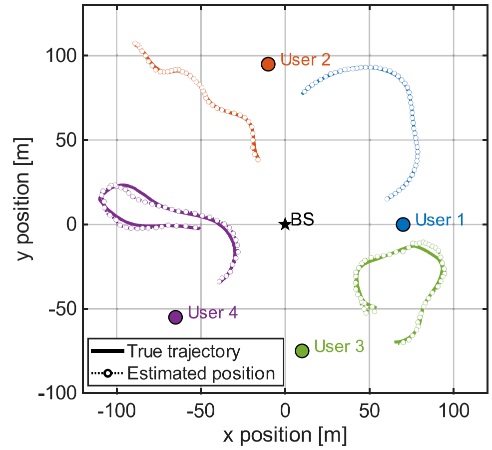

Fig. 1. Simulated sensing scenario with four moving sensing targets. Solid curves represent the true trajectories, and dotted curves with hollow markers represent the estimated positions.

To evaluate the sensing accuracy and reliability of different resource allocation schemes, Fig. 2 shows the cumulative distribution function (CDF) of the sensing position error for all sensing targets. It can be observed that Scheme 1 achieves the lowest sensing error among all compared schemes. In particular, most of the position errors under Scheme 1 are concentrated within a small error range, demonstrating improved tracking stability. Compared with Scheme 2, Scheme 1 further reduces the sensing error by incorporating predictive future sensing value instead of relying only on instantaneous sensing value. In contrast, Scheme 3 and Scheme 4 show much wider error distributions, suggesting that non-predictive or non-value-oriented resource allocation is less effective in maintaining accurate sensing performance under time-varying target motion and measurement noise.

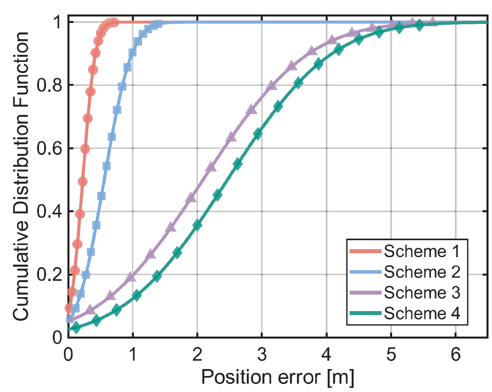

Fig. 2. Cumulative distribution function of the sensing position error under different resource allocation schemes.

Fig. 3 illustrates the sensing error as a function of the number of available radio resource blocks. For all allocation schemes, the sensing error decreases as more radio resource blocks are provided, since additional resources reduce the measurement uncertainty and improve the tracking accuracy.

Scheme 1 consistently achieves the lowest sensing error over the whole resource range. Specifically, when the number of radio resource blocks is around 20, Scheme 1 features a sensing error of about 0.7 m, whereas Scheme 2 still has an error close to 1.0 m. Scheme 3 and Scheme 4 show even larger errors, approximately 1.5 m and 2.8 m, respectively.

Scheme 1 shows a clear advantage in the limited-resource regime. It achieves a sensing error below 1 m with fewer than 20 radio resource blocks, whereas Scheme 2 requires about 30 blocks and Scheme 3 requires more than 45 blocks. Scheme 4 needs an even larger resource budget to reach comparable accuracy. Although all schemes improve as more resources are available, Scheme 1 maintains the lowest error floor, around 0.3 m, demonstrating its superior sensing accuracy and resource efficiency.

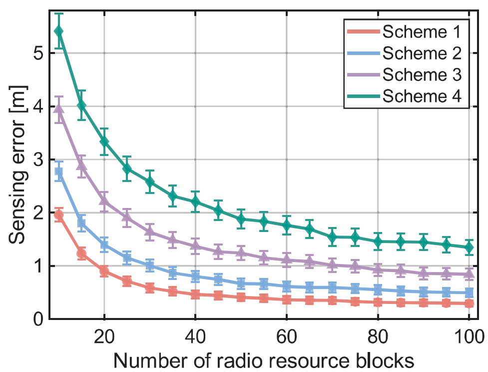

Fig. 3. Sensing error versus the number of radio resource blocks under different resource allocation schemes.

Fig. 4 compares the resource utilization efficiency of different sensing resource allocation schemes. Scheme 1 shows the highest median efficiency and a wider distribution concentrated at larger efficiency values, indicating that it can achieve better sensing accuracy with fewer radio resource blocks. In contrast, Scheme 2, Scheme 3, and Scheme 4 exhibit progressively lower efficiency, since they do not fully exploit the predictive sensing value when allocating limited resources. This result further confirms that Scheme 1 improves not only sensing accuracy but also the efficiency of resource usage.

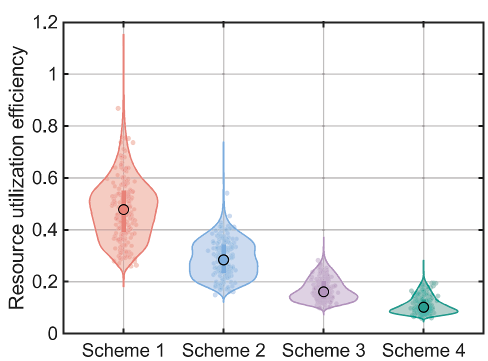

Fig. 4. Violin plot of resource utilization efficiency under different sensing resource allocation schemes.

V. Conclusion and Future Work

In this paper, a PM-VoS based resource allocation framework has been proposed for dynamic wireless sensing. The proposed framework quantifies the long-term marginal sensing utility of current sensing actions by comparing sensing-enabled and sensing-disabled covariance evolution over a finite prediction horizon. Based on this metric, a hybrid resource allocation algorithm has been developed, enabling predictive and utility-aware sensing resource allocation. The results indicate that instantaneous uncertainty alone is insufficient for dynamic sensing resource allocation, since the future covariance evolution and requirement-dependent utility saturation can change the marginal value of sensing. The proposed method still depends on the accuracy of the EKF covariance model, the representativeness of offline generated training data, and the discretization of candidate resource blocks. Future work will consider online residual-model adaptation, adaptive resource-block generation, and real-world validation with measured trajectories and channel observations. This scheme can be further extended to integrated sensing, communication, and computation systems.

References

[1] Y. Hu, Q. Jia, Y. Yao, Y. Lee, M. Lee, C. Wang, X. Zhou, R. Xie, and F. R. Yu, "Industrial internet of things intelligence empowering smart manufacturing: A literature review," *IEEE Internet Things J.*, vol. 11, no. 11, pp. 19 143–19 167, 2024.

[2] P. S. Farahsari, A. Farahzadi, J. Rezazadeh, and A. Bagheri, "A survey on indoor positioning systems for iot-based applications," *IEEE Internet Things J.*, vol. 9, no. 10, pp. 7680–7699, 2022.

[3] Y. Yang, M. Chen, Y. Blankenship, J. Lee, Z. Ghassemlooy, J. Cheng, and S. Mao, "Positioning using wireless networks: Applications, recent progress, and future challenges," *IEEE J. Sel. Areas Commun.*, vol. 42, no. 9, pp. 2149–2178, 2024.

[4] S. Saleh, S. Dwivedi, R. Whiton, P. Hammarberg, M. F. Keskin, J. Equi, H. Chen, F. Munier, O. Eriksson, F. Gunnarsson *et al.*, "Vehicular wireless positioning–a survey," *IEEE Commun. Surv. Tutor.*, 2026.

[5] B. Li, X. Wang, Y. Xin, and E. Au, "Value of service maximization in integrated localization and communication system through joint resource allocation," *IEEE Trans. Commun.*, vol. 71, no. 8, pp. 4957–4971, 2023.

[6] B. Li, X. Wang, and F. Fang, "Maximizing the value of service provisioning in multi-user isac systems through fairness guaranteed collaborative resource allocation," *IEEE J. Sel. Areas Commun.*, vol. 42, no. 9, pp. 2243–2258, 2024.

[7] B. Li and X. Wang, "Opportunistic reuse of spatial-temporal resources in multi-user isac systems for value of service maximization," *IEEE Trans. Wireless Commun.*, 2025.

[8] B. Hua, H. Peng, Z. Li, N. Cheng, K. Zhang, and Z. Su, "Joint dynamic tracking and robust secure beamforming for full-duplex isac systems," *IEEE Transactions on Wireless Communications*, vol. 25, pp. 8614–8628, 2025.

[9] Z. Zheng, Q. Wu, Y. Zhu, W. Chen, Y. Gao, and H. Wang, "Wireless sensing with movable intelligent surface," *IEEE Journal of Selected Topics in Signal Processing*, pp. 1–16, 2026.

[10] B. Li, X. Wang, E. Au, and Y. Xin, "Joint localization and environment sensing of rigid body with 5g millimeter wave mimo," *IEEE Open J. Signal Process.*, vol. 4, pp. 117–131, 2023.

[11] Y. Yuan, G. Qin, D. Li, M. Zhong, Y. Shen, and Y. Ouyang, "Real-time joint filtering of gravity and gravity gradient data based on improved kalman filter," *IEEE Trans. Geosci. Remote Sens.*, vol. 62, pp. 1–12, 2024.

[12] V. Nasteski, "An overview of the supervised machine learning methods," *Horizons. b*, vol. 4, no. 51-62, p. 56, 2017.

[13] F. Amirghafouri, A. A. Neghabi, H. Shakeri, and Y. E. Sola, "Nature-inspired meta-heuristic algorithms for resource allocation in the internet of things," *Int. J. Commun. Syst.*, vol. 38, no. 5, p. e6141, 2025.